TITLE

Preservation of autogenic processes and allogenic forcings within set-scale aeolian architecture I: numerical experiments

AUTHORS

Swanson[1*], T., D. Mohrig[2], G. Kocurek[2], B. T. Cardenas[2], M. A. Wolinsky[3]

[1] *Department of Earth, Environmental and Planetary Sciences, Rice University, MS-126*

6100 Main Street, Houston, TX 77005 USA

[2]*Department of Geological Sciences, Jackson School of Geosciences, The University of Texas at Austin, 1 University Station C1100, Austin, TX 78712 USA*

[3]*Independent researcher, Houston, Texas*

[*] Corresponding author: *ts42@rice.edu*

ABSTRACT

A reduced complexity aeolian dune stratification model is developed and applied to explore the role of dune morphodynamics in the creation of synthetic sections of aeolian stratigraphy originating from three sets of environmental forcing: 1) steady wind transport capacity, 2) steady bed aggradation and variable wind transport capacity, and 3) steady wind transport capacity and bed aggradation. In each scenario, the forward motion of initial, highly disorganized dunes generates a significant record exclusively containing autogenic signals that arise from early dune growth, deformation, and merger. However, continued dune growth scours deeply, and shreds all records of early dunes. Afterward, dunes self-organize into quasi-stable groups. Forward motion of dune groups create, truncate, and amalgamate sets and co-sets of

cross-strata, quickly forming a second, significantly more robust stratigraphic record, which preserves a comingling of signals sourced from ongoing autogenic processes and each scenario's specific set of environmental forcings, the allogenic boundary conditions of the sand sea. Although the importance of self-organization on modeled aeolian stratification is clear in the few presented scenarios, self-organization may be throttled via variability within environmental forcings, as thoroughly documented within a companion paper Cardenas et al. (This issue). Therefore, additional work is warranted as this numerical experiment only begins to sample possible sets of environmental forcing, boundary conditions, and initial conditions, geomorphic responses, and consequential preservation possible within the presented surface-stratigraphic dune modeling framework.

KEYWORDS (5)

Aeolian, dune, stratigraphy, exploratory model, self-organization

INTRODUCTION

Aeolian dune fields emerge and form patterns by autogenic processes operating within a set of allogenic boundary conditions, which, broadly speaking, are ultimately derived from climatic, tectonic, and base-level basin-scale processes (Kocurek, 1999; Jerolmack and Paola, 2010; Rodríguez-López et al., 2014). A fundamental challenge of stratigraphy, and a common task of workers is to unravel the interplay of autogenic and allogenic signals frozen within sections of aeolian sedimentary rock to reconstruct the morphology of ancient dunes and the allogenic conditions that existed within the ancient environment (Eastwood et al., 2012). However, within a dry sand sea composed of readily erodible sediments, the tumultuous motion of dunes may cause punctuated, non-uniform scouring and filling within the sediment accumulation, plausibly cannibalizing previously deposited material and shredding environmental signals. To explore the interplay of autogenic and allogenic processes, and incompleteness of the aeolian rock record, a reduced complexity model of bedform strata-formation is extended from extant models of bedform topography (Jerolmack and Mohrig, 2005a; Swanson et al., 2017) and applied to explore the role of dune morphodynamics in the creation of a synthetic aeolian rock record and shredding of environmental signals originating from three sets of allogenic boundary conditions. In a companion article within this issue, Cardenas et al., (Companion), present detailed mapping of set-scale architecture of the Jurassic Page Sandstone which is used to similarly parse the relative contributions of competing autogenic and allogenic processes.

The creation and preservation of an aeolian rock record relies on several environmental factors. Firstly, sufficient sediment must be made available and transported to allow for sand sea construction. Secondly, sediment accumulation occurs if appropriate spatial and temporal changes in sediment transport capacity allow for the formation of a sedimentary body. And finally, accommodation is needed to preserve this sediment accumulation (Kocurek, 1999). Environmental signals encoded within the aeolian rock record arise from changes in external forcings, i.e. the allogenic boundary conditions of the sand sea, such as sediment supply and annual cyclicity of sediment transporting wind (Rubin, 1987; Eastwood et al., 2012; Ping et al., 2014; Courrech du Pont et al., 2014; Swanson et al., 2016), and areal extent of sand sea development (Ewing and Kocurek, 2010). Although direct linkages between changes in environmental forcing and dune pattern response are not entirely understood, an unsteady external forcing is thought to drive geomorphic responses (Ewing and Kocurek, 2010), such as changes in dune size, shape, spacing, and motion, which, if preserved, are encoded as spatially variation in the geometry and arrangement of inclined strata and truncation surfaces that make up aeolian architecture.

Recent studies have identified architectural elements within aeolian sections that arise from dune autogenic processes known as bedform interactions (Brothers et al., 2017; Day and Kocurek, 2017): the way individual bedforms collide, merge, split or otherwise interact within the context of dune pattern formation (Kocurek et al., 2010). Although representing only a subset of unsteady dune motion imparted by dune processes, this substantial progress toward linking autogenic dune processes to aeolian stratigraphy highlights a need for tractable hypotheses that provide workers with testable linkages between autogenic and allogenic processes, and the aeolian rock record (Rodríguez-López et al., 2014). Ideally, these hypotheses would arise from observing modern dune fields and their recent deposits (Brothers et al., 2017). However, due to the vast time and spatial scales of aeolian systems, a viable alternative is to implement a forward model of bedform stratification to explore the roles of dune morphodynamics and environmental forcing in the creation of a synthetic aeolian rock record. However, limitations exist within prior forward models of bedform stratigraphy. For example, while the geometric model of Rubin (1987) provides workers with a tool to forward model aeolian architecture arising from the motion of dunes using an interpreted or assumed dune morphology, it does not include autogenic or allogenic processes. Similarly, the bedform stratification model of Jerolmack and Mohrig (2005b) uses a continuum granular flow model to reproduce stratigraphy that arises from the forward motion of deforming bedforms, but does not resolve initial bedform growth, nor geomorphic response to changes in environmental forcing. Therefore, a reduced complexity model of one-dimensional (1D) bedform topography is modified to create two-dimensional (2D) vertical sections of synthetic stratigraphy that encode information from both autogenic processes and imposed allogenic conditions. This surface-stratigraphic model is used to conduct a set of numerical experiments, varying (allogenic) boundary conditions of transport capacity and bed aggradation. The experimental results suggest that the earliest record of dune field growth is eroded by continued dune (autogenic) self-organization into long-wavelength, low amplitude groups. After group formation, rates of dune self-organization wane, processes operating within the dune field become sensitive to environmental forcing, and comingled autogenic and environmental signals propagate into the synthetic rock record.

METHODS

Bedform Strata-formation Model

The bedform strata-formation model adopts the bedform surface modeling strategy of Jerolmack and Mohrig (2005a) and Swanson et al. (2017), which casts bedform growth and motion as the deformation of a dynamic boundary between sediment and its transporting fluid, but does not resolve the fluid flow field. The motion of this boundary is driven by morphodynamic feedbacks between bedform topography, η, bed shear stress, τ_b, and saturated sediment flux, q_s. This feedback is formed by (1) casting q_s as a power law function of τ_b (Meyer-Peter and Müller, 1948), (2) expressing τ_b as a function of η, and (3) calculating temporal change in η as a consequence of spatial change in q_s. This system reproduces the fundamental morphodynamic behavior of bedforms including growth, interaction, and eventual self-organization to a dynamic equilibrium bedform morphology. Additionally, the system reproduces the scaling of topographic roughness through space and time seen in natural fluvial (Jerolmack and Mohrig, 2005a) and aeolian dunes (Swanson et al., 2017). Because the bedform surface modelling strategy adopted by Jerolmack and Mohrig (2005a) and Swanson et al. (2017) has proven to provide a robust characterization of dune autogenic processes, it is an ideal tool to explore the coevolution of bedform topography and stratigraphy under various environmental forcings.

The original bedform modeling framework presented by Jerolmack and Mohrig (2005a) is here modified to evolve both topography and stratigraphy driven by two allogenic boundary conditions: sediment transport capacity and bed aggradation rate. In this paper, a total of three scenarios are explored, each comprised of three deposodes, each of which is herein defined as an individual episode of deposition of duration 2.5×10^4 times steps, yielding a total simulation time of 7.5×10^4 timesteps per model scenario. The first scenario simulates bedform growth from a roughened sandy bed with steady sediment transport capacity, $\tau_{a_j} = 0.3$, and zero bed aggradation, $r_a = 0$. The second scenario includes deposodes comprised of a single period of sinusoidal variation ($\Delta\tau_a$ = 20%) of transport capacity combined with a steady bed aggradation rate, $r_a = 5\times10^{-5}$. This environmental forcing is chosen to conceptualize an aeolian system subjected to relative increases and decreases in wind strength over climate oscillations resulting in waxing and waning transport capacity (Kocurek, 1999). To complete the numerical experiment, a third scenario considers steady sediment transport capacity and constant bed aggradation, $r_a = 5\times10^{-5}$.

During each simulation, conservation of sediment is approximated by a finite volume method. The procedure adopted to solve the bedform surface evolution equation closely follows the original method presented by Jerolmack and Mohrig (2005a). All simulations use the same set of parameters listed in Table 1 unless otherwise indicated. At each time step boundary shear stress, τ_b, is computed for each node as a generic expansion of topography (Jerolmack and Mohrig, 2005a),

$$\tau_{b_i} = \tau_{a_j}\left(1 + A(\eta_i - \eta_{a_j}) + B\left(\frac{\eta_i - \eta_{i-1}}{\Delta x}\right)\right). \qquad (1)$$

For simulations 2 and 3, the cumulative sediment added during previous timesteps, $\eta_{a_j} = j\, r_a$, is removed from the boundary shear stress calculation, otherwise, each time step would cause global increases in boundary shear stress. The practice of expressing boundary shear stress as a function of topographic height and slope is deeply rooted in early studies of fluid motion over bedform topography (Exner, 1925). However, boundary shear stress is also found to scale with the aspect ratio of bedforms, $\tau_b \propto h\lambda^{-1}$, where h and λ are the height and wavelength of a bedform (Jackson and Hunt, 1975; Kroy et al., 2002). Therefore, any increase in bedform crest height or surface slope, will create a proportional increase in boundary shear stress over the stoss slope of the bedform. This fundamental behavior of total boundary shear stress increasing with flow blockage and shoaling are described by shape parameters A and B, respectively (Jerolmack and Mohrig, 2005a). The boundary shear stress-topography relationship approximates the along stoss slope trend in boundary shear stress derived from sediment flux over a stoss slope of an aeolian dune observed by Lancaster et al. (1996). To approximate the transport conditions within a lee shadow zone, nodes with boundary shear stress less than zero are set to zero,

$$\tau_{b_i} = \begin{cases} \tau_{b_i}; \tau_{b_i} > 0 \\ 0; \tau_{b_i} \leq 0 \end{cases}, \qquad (2)$$

as boundary shear stress along a lee slope is always computed as negative (Jerolmack and Mohrig, 2005a). Closely following the bedform modeling strategies of Diniega (2010), Jerolmack and Mohrig (2005a), and Hersen (2004), lee slopes that exceed a threshold angle, $\theta_c = 32°$, relax via an down-wind calculated diffusion, written as

$$q_{a_i} = \begin{cases} E\left(\left(\frac{\eta_i - \eta_{i+1}}{\Delta x}\right)^2 - \tan{\theta_c}^2\right)\left(\frac{\eta_i - \eta_{i+1}}{\Delta x}\right) & ; \text{atan}\left(\frac{\eta_i - \eta_{i+1}}{\Delta x}\right) \geq \theta_c. \\ 0; \text{atan}\left(\frac{\eta_i - \eta_{i_{i+1}}}{\Delta x}\right) < \theta_c & \end{cases} \quad (3)$$

A large avalanching coefficient $E = 20$ is chosen so that lee slopes relax by an avalanche flux, q_{a_i}, to an angle of repose in approximately single time step (Jerolmack and Mohrig, 2005a; Diniega, 2010). Lee slopes below the threshold angle do not trigger the calculation of avalanche fluxes (Eq. 3). The magnitude of all fluxes, q_{s_i} is then computed for each node as $q_{s_i} = m\tau_{b_i}^n + q_{a_i}$. Sediment flux is computed using the local values of boundary shear stress using the power-law relationship of Meyer-Peter and Müller (1948) with a coefficient, $m = 1$ and exponent, $n = 3/2$ (Jerolmack and Mohrig, 2005a). The chosen power-law relationship is comparable to the ballistic formula of Bagnold (1941) and was chosen to represent saturated sediment flux over bedform topography (Kroy et al., 2002). The elevation change at each node is calculated by,

$$\Delta\eta_i = \frac{-\Delta t}{(1-p)\Delta x}\left(q_{s_i} - q_{s_{i-1}}\right) + \frac{\Delta t D}{(\Delta x)^2}\left(\eta_{i+1} + \eta_{i-1} - 2\eta_i\right) + r_j, \qquad (5)$$

which combines a first order upwind finite difference of sediment flux q_{x_i}, accounting for porosity, p, with a first order approximation of topographic diffusion with diffusivity D. Topographic diffusion is superimposed for enhanced numerical stability (Press et al., 1996; Jerolmack and Mohrig, 2005a).

Table 1

Model Grid, Boundary, and Initial Conditions

The 1D model domain is composed of 1001 nodes with uniform spacing Δx. A periodic boundary condition is formed by allowing the first and last nodes to exchange sediment as if contiguous. This boundary condition allows bedforms to repeatedly cycle through the domain, which represents the temporal evolution dunes within an interior portion of a dry sand sea, where sediment accumulation and eventual preservation are likely to occur in natural settings. All runs are initialized with a roughened bed of low amplitude random topography uniformly distributed about a mean of 0.1. Different initial conditions yield different topographic fields for the same model scenario, and therefore create different stratigraphy. To sample model dependence on the initial bed topography, an ensemble of model results are obtained for each scenario by running a set of 12 realizations of initial bed topography, resulting in a total of 36 runs. Ensembles of results allow for signal averaging, which is a time domain signal processing technique that strengthens signals relative to noise, which in this case, noise could be conceptualized as the model dependence on initial bed topography. Larger ensembles of initial conditions and model runs were explored; however, a set of 12 initial conditions was found to adequately sample the variability in topography and stratigraphy that arises from specific initial bed configurations. However, for consistency, all presented stratigraphic sections are generated using the sixth initial condition of bed topography from the set of twelve initial conditions used to generated ensembles of simulation results.

Topographic and Stratigraphic Post-Processing

Post-processing of both topography and stratigraphy is performed at specified time intervals. To capture rapid changes during early simulation time, model time steps are post-processed every $100\Delta t$ for $t < 5000\Delta t$. Afterward, to reduce computational cost, this interval is increased to $700\Delta t$, resulting in a total of 200 samples per run. For each sample, consecutive pairs of dune crest and trough elevation are identified and differenced to calculate dune height, h; likewise, dune-trough positions are differenced to calculate dune wavelength, λ. A stratigraphic section is then constructed using all timesteps of dune topography up to the time step of interest. Afterward, the elevation of all erosional surfaces, otherwise known as bounding surfaces, are identified within the section. For each sample, the cumulative number of dunes that have passed each grid node and the number of bounding surfaces above each node are counted. Successive bounding surface elevations are differenced vertically to calculate the thickness of sets of cross-strata, which are herein referred to as set and set thickness, l_{st}. Any set with $l_{st} < 0.01$ is discounted, as it is unlikely that such a thin unit will be identified as an independent set of cross-strata in actual sedimentary deposits. Additionally, in analyses that relate distributions of dune height to distributions of l_{st}, dune heights are filtered to only include events that occur after the creation of the earliest bounding surface within each stratigraphic section.

To facilitate comparison with physical systems, the vertical, horizontal, and time scales of modeled stratigraphic sections are nondimensionalized by the dynamic equilibrium values of dune height, wavelength, and deposode period, respectively; creating nondimensionalized elevation, $\eta^* = \frac{\eta}{h_{eq}}$, horizontal distance, $x^* = \frac{x_i}{\lambda_{eq}}$, and simulation time, $t^* = \frac{\sum_j \Delta t}{2.5 \times 10^4 \Delta t}$. For each run, h_{eq} and λ_{eq} are found by a non-linear least squares fitting of the model, $s(t^*) = s_{eq}\left(1 - e^{-at^*}\right)$, where the variables s and s_{eq} represent the time-series and dynamic equilibrium values of the morphological scale of interest, respectively. Deposode period is obtained from the wavelength of τ_a in scenario 2. This practice places model results in a conceptual reference frame of equilibrium dune morphology and deposode duration.

RESULTS

Dynamic Dune Scales

During early simulation time, scenarios show similar temporal changes in spatially and ensemble averaged dune height, $\bar{h}$, and dune wavelength, $\bar{\lambda}$ (Figs. 1A, B). Throughout the simulation, $\bar{h}$ is measured as the vertical distance between the spatially and ensemble averaged dune crest and trough elevations (Fig. 1C), and $\bar{\lambda}$ is dune crest to crest horizontal distance. Starting from the initial condition, each simulation exhibits a brief duration of very slow change in bed configuration (Figs. 1A, B). This corresponds to low values of sediment flux and boundary shear stress computed along initial low-lying topography (Eq. 1). Gradually, low amplitude bedforms self-organize from initial bed roughness, slowly increase in size, and begin to coalesce. After initial growth and coalescence, $\bar{h}$ and $\bar{\lambda}$ rapidly increase, then saturate, reaching a dynamic equilibrium by $t^* \approx 0.2$ (Figs. 1A, B). After reaching dynamic equilibrium, dune $\bar{h}$ and $\bar{\lambda}$ begin to respond to the set of environmental forcings unique to each scenario. For example in scenarios 1 and 3, which do not include time varying values of τ_A, dunes exhibit exponential growth, then saturation to an equilibrium morphology; a characteristic response of bedforms evolving under steady unidirectional flows (Baas 1994) (Fig. 1A). In contrast, after initial growth, dunes in scenario 2 responds to sinusoidal variation in τ_A with a similar sinusoidal oscillation about an equilibrium value of $\bar{h}$ (Fig. 1A). Notably, the equilibrium value of $\bar{\lambda}$ is significantly larger in scenario 2, but relatively insensitive to fluctuations in τ_A (Fig. 1B). In strong contrast to mean dune scales, for each scenario, the time series of the standard deviation of ensemble dune height, σ_h, is nearly identical throughout all simulation time. At first, σ_h rapidly increases to a maximum value at approximately $t^* \approx 0.1$. Afterward, at first, σ_h decreases at a rapid rate, then at approximately $t^* \approx 0.2$, the slope of σ_h decreases slowly for the remainder of simulation time.

Figure 1

Topographic and Stratigraphic Co-evolution

Early Simulation Time.---As with early changes in mean dune scales, stratigraphic sections during the initial stages of bedform growth and merger in each scenario are nearly identical. Within the first hundredths of a deposode, bedforms spontaneously emerge from the rough sandy bed and develop internal stratification. At this time, dunes exhibit significant morphological variability, underscored by differences in height, wavelength, and the crest and trough elevations (Figs. 1D,2A). Due to this variability, these early dunes differ in celerity, allowing dunes to collide and merge. In these early timesteps, individual dunes increase in size by scouring into bed material below initial bed elevation (dunes on left and right side, Fig. 2), and from dune merger (left side, Figs. 2B, C). Occasionally, dune-troughs may scour through the stoss surfaces of down-wind dunes, creating new truncation surfaces, and new cross-sets with significant thickness, which can approach the height of individual dunes. This newly created stratigraphy is laterally discontinuous, but in places contains a substantial record of early dune self-organization. For example, portions of the domain document the passage of multiple dunes, as indicated by multiple, vertically stacked bounding surfaces (middle region, Fig. 2C).

Figure 2

After initial dune coalescence, continued dune growth is sustained by rapid scouring of bed materials (Fig. 1C) and consequent cannibalization of the earliest synthetic rock record in all scenarios (Fig. 3A). Across the domain, dune-troughs descend nonuniformly, creating self-organized groups of dunes with higher troughs and groups with lower troughs (arrows, Fig. 3A). Further dune growth ceases as troughs descend significantly below mean bed elevation, and τ_b becomes vanishingly small, which leaves substantial spatial variations in scour depth and individual-dune celerity throughout the domain. Afterward, spatial variations in scour depth propagate in the transport direction at a group celerity. Trough motion imparted by group celerity occurs in the same direction as individual dune motion, is achieved by the same morphodynamic feedback (Equations 1 through 5), simply manifesting as a long wavelength (~ $5\lambda_{eq}$ to $10\lambda_{eq}$), low amplitude (~ $0.1h_{eq}$ to $0.2h_{eq}$) variation in bed elevation (Fig. 4). However, the motion of dune groups is accomplished by way of routing sediment through individual dunes. Within a dune group (Fig. 4), upwind dunes are arranged in increasing elevation in the down-transport direction. Due to these consecutive increases in elevation, each dune experiences more total boundary shear stress (Eq. 1 *A*-term) and scours more vigorously compared to its upwind neighbor. This ultimately causes deflation of the upwind portion of the dune group and routes an excess of sediment through ascending dunes toward the leeward portion of the dune group. Along the leeward segment, each consecutive dune is slightly lower in elevation (Fig. 4). Because of this, each down-wind dune receives more sediment than it can transport over its stoss slope. By conservation, this causes dunes on the leeward portion of the dune group to ascend.

Therefore, through the paired motion of scouring upwind dunes and ascending leeward dunes allows the dune group to move forward. Therefore, after the formation of dune groups (Fig. 3A), lower dune-troughs ascend (Fig. 3B), and begin to create a substantial record (arrows, Fig. 3C). The lowest erosional surface shown in Figure 4C represents the furthest descent of dune-troughs and the lowest portion of initial dune groups. This scour depth is never revisited, and represents the lowest bounding surface in all model scenarios.

Figure 3

Long-Term Topographic and Stratigraphic Co-evolution.---In each scenario, immediately after group formation, the passage of individual dune-troughs within groups create co-sets (Figs. 4C, 5). Within a dune group, dune-troughs at the lowest portion of a dune group are slowly carried upward as the dune group moves forward, as group celerity is faster than individual dune celerity. This combined motion of dune-troughs within dune groups produces individual sets that start near zero thickness near the bottom of a co-set, and typically show upward increases in bounding surface slope and thickness until terminating into a modern dune (annotated dune group, Fig. 4), or bounding surface. As dunes continue to self-organize, dune-trough elevation variability decays with simulation time, as indicated by decreases in σ_h (Fig. 1D). Within all sections, this decay in dune disorder is recorded within the architecture of the synthetic sections as an upward transition from co-sets composed of a few, large sets separated by steep bounding surfaces toward sub-horizontal bounding surfaces, and more numerous, thinner sets packaged within later co-sets (Figs. 4,5,6,7). However, the exact way this autogenic signal of self-organization is presented within synthetic stratigraphy is unique to each scenario. Many of the observations within this section are based on videos that show the longer-term ($t^* = 0.2$ to 3) co-evolution of dune topography and stratigraphy. Although only the final synthetic sections are shown below, video files of each scenario are available in supplementary materials.

Figure 4

The final stratigraphic section of scenario 1 shows architecture generated from allogenic boundary conditions of steady transport capacity, zero net bed aggradation, and autogenic self-organization of dunes within dune groups (Fig. 5). During deposition, the deepest dune-trough within each group varies between groups, and changes with simulation time due to ongoing self-organization. This spatially and temporally variable group-scour depth causes frequent lateral truncation of group-deposited co-sets that dominate the architecture present in Figure 6. Although highly compartmentalized within laterally truncated co-sets, generally, set thickness and bounding surface slope decrease, and number of sets per co-set increase upwards through the section (Fig. 5). A video showing the coevolution of dune topography and stratigraphy is available in supplementary materials (scenarioOne.mp4).

Figure 5

Despite allogenic boundary conditions of steady bed aggradation and substantial sinusoidal fluctuations in ambient boundary shear stress, all records of initial dune growth and motion are cannibalized within the final synthetic section of Scenario 2 (Fig. 6). However, as τ_a increases during periodic fluctuations, sediment transport rates increase, which allows dune-troughs to scour deeper, driving an increase in $\bar{h}$ (Fig. 1A,C). During increases in τ_a, the scouring action of dune groups outpaces trough elevation gain associated with the overall aggradation of the bed (Fig. 1C). The rhythmic motion of dune-trough decent and ascent with waxing and waning τ_a drives amalgamation of sets into nearly laterally continuous bounding surfaces with significant undulations in elevation (Fig. 6). Similarly, the ascent and descent of dune-troughs form large-scale undulations in the thickness of both individual sets and co-sets (Fig. 6). Although comingled with changes imparted by fluctuated transport capacity, individual set thicknesses and bounding surface slopes generally decrease, and the number of sets within a co-set generally increase up-section. A video showing the coevolution of dune topography and stratigraphy is available in supplementary materials (scenarioTwo.mp4).

Figure 6

In scenario 3, like scenario 2, despite constant bed aggradation, the earliest records are cannibalized by dune self-organization and group formation (Fig. 7). However, in strong contrast to sections generated by scenarios 1 and 2, group-deposited co-sets appear vastly more tabular, and extend across the entire section. Within Figure 8, the upward transition from a few, thick, highly inclined sets within each co-set toward co-sets containing numerous, thin, sub-horizontally inclined sets generated by the ongoing self-organization of dune-troughs within dune groups is exceptionally clear. A video showing the coevolution of dune topography and stratigraphy is available in supplementary materials (scenarioThree.mp4).

Figure 7

Fractional Dune Preservation.---Within the first hundredths of a deposode ($t^* \approx 0$ to 0.05), initial topography is rapidly worked into low lying, disorganized bedforms (Fig. 1). Their forward motion causes a notable increase in the average number of dunes that have visited each grid node, n_d (Figs. 8A,B), and average number of sets at each grid node, n_s (Figs. 2,8C,D). Likewise, fractional dune preservation, $\kappa = n_s n_d^{-1}$, increases to a local maximum (Fig. 8E). Immediately afterward, precipitous declines in n_d, n_s, and κ (Figs. 8B,C,E) coincide with continued dune growth (Fig. 1A), dune merger (Fig. 2), and amalgamation of sets (Fig. 3A). Next, by $t^* \approx 0.1$, the forward motion of non-uniform dune-trough elevations within dune groups begins to create new sets (Figs. 4B,C), which correlate to rapid increases in n_d, n_s, and κ (Figs. 8A,C,E). From thereon, in each scenario, n_d increases at a nearly constant rate (Fig. 8B). Conversely, set creation by forward motion of dune groups shows significant variability between scenarios and over the remainder of each scenario (Fig. 8D). For the zero-aggradation case, scenario 1, n_s increases monotonically with a gradually decreasing slope (Fig. 8D). In the case of scenario 2, n_s oscillates about a generally increasing trend. However, in scenario 3, which includes constant aggradation, n_s increases monotonically and exhibits a gradual, but continuous increase in slope (Fig. 8D). In all scenarios, κ increases rapidly until $t^* \approx 0.2$; beyond which, κ shows marked differences. During the remainder of scenario 1, κ decays slowly, suggesting fewer dunes are preserved with increasing simulation time (Fig. 8E). Conversely, in scenario 3, κ decreases at first, then past one deposode, begins to increase slowly for the remainder of simulation time (Fig. 8E). Despite periodic perturbation by waxing and waning τ_a in scenario 2, dune-trough elevation variability decay combined with constant aggradation allows more, but thinner sets to be preserved by pulsating dune groups (Fig. 6), this behavior gives κ strong oscillations superimposed on a trend similar to scenario 3 (Fig. 8E).

Figure 8

Dune Height and Set Thickness Distributions.---During each simulation, topography and stratigraphy are sampled to obtain growing populations of dune height and set thickness. The distribution of each sample population of dune heights is described using the coefficient of variation, $c_v = \sigma_h \mu_h^{-1}$ (Fig. 9A), where σ_h and μ_h are the standard deviation (Fig. 1D) and mean values of dune height (Fig. 2A) calculated using estimates of shape and rate parameters from maximum likelihood gamma distribution fits. Immediately after the first timestep, c_v rapidly increases to its maximum value at $t^* \approx 0.04$. This occurs in all scenarios, and corresponds to initial working of a rough bed into the earliest, least organized dunes, as indicated by high values of c_v (Figs. 3,10A). Afterward, during rapid dune growth, c_v decreases quickly until individual dunes are organized in to groups, at $t^* \approx 0.2$ (Fig. 9A). After this precipitous decrease, generally, c_v gradually decreases for the remaining simulation time (Fig. 9A). Notably, however, scenario 2 shows faint oscillation, and maintains slightly larger values of c_v compared to scenarios 1 and 3 (Fig. 9A). Similarly, mean set thickness, μ_{st}, estimated from maximum likelihood exponential distribution fits, shows a dramatic increase, obtaining a maximum value just after initital formation of dune groups at $t^* \approx 0.1$ (Fig. 9B). Afterward, μ_{st} generally declines with simulation time. However, during later simulation time, scenario 2 and 3 tend to have larger values of μ_{st}, which is attributable to constant agradation. However, scenario 2 maintains the largest values of μ_{st}, which oscilate in response to changes in dune-trough elevation driven by fluctuations in τ_a (Fig. 9B). At first, the preservation ratio, $\omega = \mu_h \mu_{st}^{-1}$ (Paola and Borgman 1991), rapidly decreases during very early simulation time (Fig. 8C), then correpsonding to the initial formation of dune groups, ω reaches a local maximum at $t^* \approx 0.1$ (Fig. 9C). Afterward, ω rapidly decays as ongoing dune group motion begins to truncate the largest sets at the lowest portion of every section (Fig. 3C). Similar to κ, after $t^* \approx 0.2$, the trajectory of ω is different from each scenario. In scenario 1 further changes in ω are very similar to κ (Fig. 9D), where ongoing decay of dune-trough elevation variability creates thinner sets upsection (Fig. 5). However, despite constant agradation, ongoing decreases in dune-trough elevation variability cause slower, but, monotonically decreasing ω for the remainder of scenario 3. Similarly, scenario 2 shows a general decrease in ω, with superimposed osciations, which correspond to subtle fluctuations in set thickness due the puctuated scour and deposition from dune groups, driven by sinusoidal fluctuations in τ_a.

Figure 9

DISCUSSION

This numerical experiment clearly shows two distinct periods of topographic and stratigraphic coevolution. In all examined scenarios, dune scale, motion, stratigraphy, and preservation are exceedingly similar during the first quarter deposode. Afterward, the characteristic rapid changes in dune morphology and motion quell, and the ongoing morphodynamic processes operating within a dune field become sensitive to changes in environmental forcing. To help identify systematic changes during the co-evolution of bedform topography and stratigraphy, the stochastic theory of Paola and Borgman (1991) is applied as a theoretical benchmark for dune preservation in each scenario.

Benchmarking Dune Preservation

Paola and Borgman (1991) envisioned set creation to arise from the passage of a train of bedforms scouring to random depths, working and re-working sediment with zero net bed aggradation. In this framework, the preservation ratio, ω, is related to the coefficient of variation of bedform height, $\omega = 1.645\ \varepsilon^{-1} c_v^2$, where the reference level, ε, is a cutoff that segments the distribution of dune height into set-creating versus non-set creating portions. In the case of Paola and Borgman (1991), ε is set equal to 2, allowing only scour below mean bed elevation to create sets. While the modeled scenarios here are markedly different from this theoretical system, the application of this stochastic framework provides a benchmark for dune preservation in the case where dune-trough elevations are randomly distributed in space and time and is referred to here as the PB theory (Fig. 10). Therefore, a reasonable supposition would be that any significant departure from this expected relationship may reflect systematic changes in bedform morphology and/or preservation, attributable to autogenic dune processes such as self-organization and/or geomorphic responses to allogenic boundary conditions.

Figure 10

Within the first hundredths of a deposode, the forward motion of small, disorganized, and rapidly deforming dunes creates populations of dune height and set thickness (Figs. 2,9C) that are in reasonable agreement with PB theory ($t^* \lessapprox 0.05$, Fig. 10). Immediately afterward, increases in scour depth (Fig. 1C), and ongoing dune merger (decline in n_d, Fig. 8A) drive increases in both μ_h and σ_h (Fig. 1). However, increases in μ_h are unevenly accommodated by changes in both dune crest and trough elevation (Fig. 1C), and outpace simultaneous increases in μ_{st} (Fig. 9B), which drives both a precipitous decline in ω (Fig. 9C), and significant excursion from PB theory ($t^* \lessapprox 0.1$, Fig. 10). During this period, the ongoing descent of dune-troughs during dune group self-organization locally amalgamates sets into bounding surfaces in an asynchronous manner, evidenced as κ never returns to zero (Fig. 8E). This duration of substantial set amalgamation effectively clears the stratigraphic memory, shreds any systematic relationship between dune topography and stratigraphy, and returns all scenarios toward temporary agreement with PB theory by $t^* \approx 0.1$ (Fig. 10). Afterward, all scenarios largely run subparallel to PB theory, with the exception of a brief increase in ω, at $t^* \approx 0.2$, which corresponds to a highly ephemeral, yet robust record created by the passage of the first dune group (Fig. 3C), which is partially cannibalized by the passage of later groups.

PB theory does not predict temporal changes between moments of dune topography and stratigraphy, yet, aside from early periods of dune growth and group formation ($t^* < 0.1$), preservation trends largely run subparallel to PB theory ($t^* > 0.1$, Fig. 10). This offset trend is interpreted as a self-organization signal, which arises from ongoing homogenization of dune-trough elevations (Fig. 9A), and consequential decreases in preservation (Fig. 9C). However, superimposed on this generalized trend are subtle changes in ω and c_v, which correspond to each set of allogenic boundary conditions. For example, the unsteady transport capacity in scenario 2 corresponds to fluctuations in ω (Figs. 10C, 11). Furthermore, scenario 2 terminates at the highest values of ω and c_v; suggesting that variability in environmental forcing helps maintain topographic variability, and consequentially, bolsters preservation. Past $t^* \approx 0.2$, the remainder of scenario 1 plots significantly below scenario 3 (Fig. 10), which is directly attributable to steady aggradation in scenario 3.

Path Forward and Error

The co-evolution of dune topography and stratigraphy produced by this model is unlikely to exactly match any specific physical analog. However, the process-based interpretations of architectural elements within the experimental sections define five primary scenarios that can be used as working hypotheses to guide the interpretation of any succession of aeolian strata. Firstly, dune growth is a spontaneous autogenic process that cannibalizes records of the youngest dunes, and therefore, shreds any early environmental record of a system. This result may help to support recent field interpretations of cannibalization of early dune deposits in the Entrada Sandstone (Kocurek and Day, 2018). However, a potentially useful corollary to this hypothesis is that confirmed preservation of early dune accumulations may be diagnostic of an external control on dune preservation, such as, water table rise, precipitation that would shutoff aeolian transport, or early dune deposition within antecedent topographic lows (Cardenas et al., Companion). Secondly, self-organization into groups of dunes, and subsequent group-based deposition of co-sets is an important process in the creation and preservation of aeolian stratigraphy. This hypothesis is comparable to preservation mechanisms proposed by previous studies which have focused on set-scale preservation occurring within nested scales of fluvial morphological elements including bars, channels, and channel belts (Miall, 2015; Reesink et al., 2015; Paola et al., 2018; Herbert and Alexander, 2018). Additionally, the forward motion of dunes within dune groups drives modest dune climb, and the scouring action of dune group troughs may create outcrop scale truncation surfaces, which within this experiment, arise from autogenic processes, but would typically be recognized as parasequences and super-surfaces, and therefore possibly thought to originate from allogenic boundary conditions. Within the Page Sandstone the passage of dune groups are thought to generate outcrop-scale bounding surfaces and intervening dune strata that climb at very low angles. This co-set architecture is interpreted to represent lowered base-level, and associated scour-and-fill architecture tied to the passage of dune groups within a dry aeolian system (Cardenas et al., Companion).

The third working hypothesis is that a dune field becomes increasingly sensitive to its set of allogenic boundary conditions as dune self-organization rates slow over time. This allows allogenic and autogenic signals to comingle and enter the aeolian rock record as the entire field matures. Fourthly, temporal changes in preservation due to self-organization provide a plausible pathway for future workers to deconvolve signals arising from dune autogenic behavior from changes in the imposed allogenic boundary conditions. For example, Cardenas et al. (Companion) observed that set thickness variability within a well-established wet aeolian system (Entrada Sandstone) is measurably less than what is expected from random scouring within a dry system such as the Page Sandstone. Finally, all numerical scenarios of set variability plot below that of the PB theory (Fig. 10), suggesting that self-organization of dunes within groups reduces preservation compared to a truly random bedform system. Although PB theory has been combined with a geometric model (Allen, 1970) to account for bedform climb (Bridge and Best, 1997), the chosen reference level, ε has been carefully modified to match experimental topography and resulting stratification (Leclair and Bridge, 2001); further work should emphasize bedform preservation under the influence of self-organization. Regardless of environment or planet, self-organization of bedforms into fewer, larger forms during bedform pattern formation is a ubiquitous process (Day and Kocurek, 2018), and therefore may have profound implications for the reconstruction of bedform topography from cross-stratified deposits.

These experimental results and interpretations are the products of mass-conserving numerical approximations for bedform topography evolution (Jerolmack and Mohrig, 2005a). Because of the heuristic nature of this model, there is no analytical solution in which to validate or otherwise constrain error that arises from the numerical treatment. However, the bedform surface model recreates the scaling behavior of natural fluvial and aeolian bedform topography and reproduces fundamental bedform morphodynamic behavior, such as, self-organized pattern development through bedform growth and interactions (Jerolmack and Mohrig, 2005a; Swanson et al., 2017). However, this bedform modeling strategy cannot simulate dune behavior associated with sediment transfer between dunes via sediment entrainment within turbulent wake (Mohrig and Smith, 1996; Swanson et al., 2018). Therefore, application and perception of this exploratory model should be tempered by its simplicity and the results of this study warrant further exploration with theoretical models, physical models, natural dune fields, and ancient aeolian rock records (Cardenas et al., Companion).

CONCLUSIONS

A one-dimensional morphodynamic model of bedform topography is adapted to create two-dimensional synthetic sections of aeolian stratigraphy arising from three different sets of allogenic boundary conditions: 1) steady transport capacity, 2) steady bed aggradation and variable transport capacity, and 3) steady transport capacity and bed aggradation. In each scenario, the initial roughened sandy bed is quickly worked into a field of small, disorganized dunes. The forward motion of these initial dunes generates a significant record exclusively containing autogenic signals that arise from early dune growth, deformation, merger, or generically described as dune self-organization. However, despite steady bed aggradation in scenarios 2 and 3, continued dune growth and self-organization into dune groups, shreds all records of early dunes in all scenarios. Shortly after group formation, dunes scales reach dynamic equilibrium, and ongoing rates of self-organization slow. Forward motion of individual troughs within dune groups create and truncate co-sets of cross-strata, quickly forming a second, significantly more robust stratigraphic record, which preserves a comingling of signals sourced from slowed self-organization and each scenario's specific set of allogenic boundary conditions. Interestingly, in all scenarios, preserved signals of self-organization are sourced from ongoing homogenization of dune-trough elevations, and consequential decreases in preservation, which is found to generally follow to a well-known stochastic theory that relates moments of bedform topography to stratigraphy.

The numerical experiments here do not explore different wind regimes, sediment supply limitations, bedform morphologies, nor the types of bedform interactions that are possible to simulate using the bedform surface modeling approach (Jerolmack and Mohrig, 2005a; Swanson et al., 2017). To encourage further exploration of the interplay between autogenic processes and different sets of allogenic boundary conditions, all model source code and post-processing routines have been extensively commented and are available at https://tswanson.net/bedform-strata-formation-model/. All figures within the manuscript are reproducible using the provided code. Parallelized model execution and post-processing of the results presented in this manuscript requires approximately 16 gigabytes of system memory and 25 minutes of execution time on a multi-core computer.

Although the importance of self-organization on modeled aeolian stratification is clear in the few presented scenarios, self-organization maybe throttled by external variability fed into the sedimentary system through allogenic boundary conditions. Therefore, additional work to explore the role of self-organization within of aeolian stratification is warranted as this numerical experiment only begins to sample possible sets of unsteady environmental forcings within allogenic boundary conditions, and initial conditions, geomorphic responses, and consequential preservation. However, self-organization of bedforms is a ubiquitous autogenic process in bedform pattern formation in all detrital systems, regardless of environment or planet, and is likely a vastly important source of autogenic signals within aeolian rock records.

ACKNOWLEDGEMENTS

This numerical experiment benefited from discussions with Man Liang, Mauricio Perillo, John Martin, Nick Howes, Ru Smith, and Caroline Hern. This work is an extension of a dissertation chapter which received vastly helpful comments and edits from Wonsuck Kim, Joel Johnson, and Paola Passalacqua, and was partially supported by Shell International Exploration & Production Inc. Additionally, the Shell Center for Sustainability at Rice University supported

a portion of this work. However, this work does not reflect the views of Shell International Exploration & Production Inc.

REFERENCES

Allen, J.R.L., 1970, A Quantitative Model of Climbing Ripples and Their Cross-Laminated Deposits: Sedimentology, v. 14, p. 5–26, doi:10.1111/j.1365-3091.1970.tb00179.x.

Bagnold, R.A., 1941, The physics of blown sand and desert dunes,: London, Methuen & Co.

Bridge, J., and Best, J., 1997, Preservation of planar laminae due to migration of low-relief bed waves over aggrading upper-stage plane beds: comparison of experimental data with theory: Sedimentology, v. 44, p. 253–262, doi:10.1111/j.1365-3091.1997.tb01523.x.

Brothers, S.C., Kocurek, G., Brothers, T.C., and Buynevich, I.V., 2017, Stratigraphic architecture resulting from dune interactions: White Sands Dune Field, New Mexico: Sedimentology, v. 64, p. 686–713, doi:10.1111/sed.12320.

Cardenas, B., Kocurek, G., Mohrig, D., Swanson, T., Hughes, C., and Brothers, S.C., Companion, PRESERVATION OF AUTOGENIC PROCESSES AND ALLOGENIC FORCINGS WITHIN SET-SCLAE AEOLIAN ARCHITECTURE II: THE SCOUR-FILL DOMINATED JURASSIC PAGE SANDSTONE, ARIZONA, USA: Journal of Sedimentary Research,.

Courrech du Pont, S., Narteau, C., and Gao, X., 2014, Two modes for dune orientation: Geology, v. 42, p. 743–746, doi:10.1130/G35657.1.

Day, M., and Kocurek, G., 2017, Aeolian dune interactions preserved in the ancient rock record: Sedimentary Geology, v. 358, p. 187–196, doi:10.1016/j.sedgeo.2017.07.009.

Day, M., and Kocurek, G. Pattern similarity across planetary dune fields: Geology, doi:10.1130/G45547.1.

Diniega, S., 2010, Modeling aeolian dune and dune field evolution [Ph.D.]: The University of Arizona, 163 p., https://search.proquest.com/docview/734722483/abstract/D0AC103CCBB541B7PQ/1 (accessed January 2018).

Eastwood, E.N., Kocurek, G., Mohrig, D., and Swanson, T., 2012, Methodology for reconstructing wind direction, wind speed and duration of wind events from aeolian cross-strata: Journal of Geophysical Research: Earth Surface, v. 117, p. F03035, doi:10.1029/2012JF002368.

Ewing, R.C., and Kocurek, G., 2010, Aeolian dune-field pattern boundary conditions: Geomorphology, v. 114, p. 175–187, doi:10.1016/j.geomorph.2009.06.015.

Exner, F.M., 1925, Uber die wechselwirkung zwischen wasser und geschiebe in flussen: Akad. Wiss. Wien Math. Naturwiss. Klasse, v. 134, p. 165–204.

Herbert, C.M., and Alexander, J., 2018, Bottomset Architecture Formed In the Troughs of Dunes and Unit Bars: Journal of Sedimentary Research, v. 88, p. 522–553, doi:10.2110/jsr.2018.28.

Hersen, P., 2004, On the crescentic shape of barchan dunes: The European Physical Journal B - Condensed Matter and Complex Systems, v. 37, p. 507–514, doi:10.1140/epjb/e2004-00087-y.

Jackson, P.S., and Hunt, J.C.R., 1975, Turbulent wind flow over a low hill: Quarterly Journal of the Royal Meteorological Society, v. 101, p. 929–955, doi:10.1002/qj.49710143015.

Jerolmack, D.J., and Mohrig, D., 2005a, A unified model for subaqueous bed form dynamics: Water Resources Research, v. 41, p. W12421, doi:10.1029/2005WR004329.

Jerolmack, D.J., and Mohrig, D., 2005b, Frozen dynamics of migrating bedforms: Geology, v. 33, p. 57–60, doi:10.1130/G20897.1.

Jerolmack, D.J., and Paola, C., 2010, Shredding of environmental signals by sediment transport: Geophysical Research Letters, v. 37, doi:10.1029/2010GL044638.

Kocurek, G., 1999, The aeolian rock record (Yes, Virginia, it exists, but it really is rather special to create one), *in* Goudie, A.S., Livingstone, I., and Stokes, S. eds., Aeolian environments, sediments and landforms, School of Geography and St Catherines's College, University of Oxford, John Wiley & Sons, p. 239–259.

Kocurek, G., and Day, M., 2018, What is preserved in the aeolian rock record? A Jurassic Entrada Sandstone case study at the Utah–Arizona border: Sedimentology, v. 65, p. 1301–1321, doi:10.1111/sed.12422.

Kocurek, G., Ewing, R.C., and Mohrig, D., 2010, How do bedform patterns arise? New views on the role of bedform interactions within a set of boundary conditions: Earth Surface Processes and Landforms, v. 35, p. 51–63, doi:10.1002/esp.1913.

Kroy, K., Sauermann, G., and Herrmann, H.J., 2002, Minimal model for aeolian sand dunes: Physical Review E, v. 66, p. 031302, doi:10.1103/PhysRevE.66.031302.

Lancaster, N., Nickling, W.G., Neuman, C.K.M., and Wyatt, V.E., 1996, Sediment flux and airflow on the stoss slope of a barchan dune: Geomorphology, v. 17, p. 55–62, doi:10.1016/0169-555X(95)00095-M.

Leclair, S.F., and Bridge, J.S., 2001, Quantitative Interpretation of Sedimentary Structures Formed by River Dunes: Journal of Sedimentary Research, v. 71, p. 713–716, doi:10.1306/2DC40962-0E47-11D7-8643000102C1865D.

Meyer-Peter, E., and Müller, R., 1948, Formulas for bed-load transport, *in* IAHSR 2nd meeting, Stockholm, appendix 2, IAHR.

Miall, A.D., 2015, Updating uniformitarianism: stratigraphy as just a set of 'frozen accidents': Geological Society, London, Special Publications, v. 404, p. 11–36, doi:10.1144/SP404.4.

Mohrig, D., and Smith, J.D., 1996, Predicting the migration rates of subaqueous dunes: Water Resources Research, v. 32, p. 3207–3217, doi:10.1029/96WR01129.

Paola, C., and Borgman, L., 1991, Reconstructing random topography from preserved stratification: Sedimentology, v. 38, p. 553–565, doi:10.1111/j.1365-3091.1991.tb01008.x.

Paola, C., Ganti, V., Mohrig, D., Runkel, A.C., and Straub, K.M., 2018, Time Not Our Time: Physical Controls on the Preservation and Measurement of Geologic Time: Annual Review of Earth and Planetary Sciences, v. 46, p. null, doi:10.1146/annurev-earth-082517-010129.

Ping, L., Narteau, C., Dong, Z., Zhang, Z., and Courrech du Pont, S., 2014, Emergence of oblique dunes in a landscape-scale experiment: Nature Geoscience, v. 7, p. 99.

Press, W.H., Teukolsky, S.A., Vetterling, W.T., and Flannery, B.P., 1996, Numerical recipes in C: Cambridge, Cambridge university press, v. 2.

Reesink, A.J.H., Van den Berg, J.H., Parsons, D.R., Amsler, M.L., Best, J.L., Hardy, R.J., Orfeo, O., and Szupiany, R.N., 2015, Extremes in dune preservation: Controls on the completeness of fluvial deposits: Earth-Science Reviews, v. 150, p. 652–665, doi:10.1016/j.earscirev.2015.09.008.

Rodríguez-López, J.P., Clemmensen, L.B., Lancaster, N., Mountney, N.P., and Veiga, G.D., 2014, Archean to Recent aeolian sand systems and their sedimentary record: Current understanding and future prospects: Sedimentology, v. 61, p. 1487–1534, doi:10.1111/sed.12123.

Rubin, D.M., 1987, Cross-bedding, bedforms, and paleocurrents: Tulsa, Okla., Society of Economic Paleontologists and Mineralogists.

Swanson, T., Mohrig, D., and Kocurek, G., 2016, Aeolian dune sediment flux variability over an annual cycle of wind: Sedimentology, v. 63, p. 1753–1764, doi:10.1111/sed.12287.

Swanson, T., Mohrig, D., Kocurek, G., and Liang, M., 2017, A Surface Model for Aeolian Dune Topography: Mathematical Geosciences, v. 49, p. 635–655, doi:10.1007/s11004-016-9654-x.

Swanson, T., Mohrig, D., Kocurek, G., Perillo, M., and Venditti, J., 2018, Bedform spurs: a result of a trailing helical vortex wake: Sedimentology, v. 65, p. 191–208, doi:10.1111/sed.12383.

FIGURE CAPTIONS

Figure 1. A) temporal changes in spatially averaged dune height $\bar{h}$, and B) wavelength $\bar{\lambda}$ with deposode fraction t^*. C) spatially averaged crest and trough elevation. Difference between upper (dune crests) and lower (dune-troughs) curves yields dune height, $\bar{h}$ (back arrow). Note bed aggradation during scenarios 2 and 3. D) standard deviation of dune height σ_h, plotted as a function of t^*. Each scenario is plotted as the ensemble average of 12 initial conditions.

Figure 2. Sequential stratigraphic sections sampled every 0.08 $t^*$from scenario 1, initial condition 6. A) Internal stratification formed from initial dune motion. B) center dunes migrate over each other forming a significant early stratigraphic record, while dunes to the left and right scour into previously unscoured bed material. C) Rightmost dunes merge, while centered dunes maintain a significant stratigraphic record. Synthetic stratigraphy is color-mapped by time of deposition, t^*. Stratigraphic vertical exaggeration = 25x, topographic vertical exaggeration = 1x.

Figure 3. Sequential stratigraphic sections showing initial dune group formation, and forward motion in scenario 1, initial condition 6. A) complete cannibalization of early dune deposits and initial formation of dune groups segmented by deeper dune-troughs (arrows). B) Fully formed dune groups cease to scour deeper than the lowest bounding surface (arrows). C) Initial forward motion of the dune group generates first co-sets from dune-troughs (arrows). Synthetic stratigraphy is color-mapped by the time of deposition, t^*. Stratigraphic vertical exaggeration = 15x, topographic vertical exaggeration = 0.2x.

Figure 4. Stratigraphic section showing co-sets arising from the passage of dune groups in scenario 2, initial condition 6. Synthetic stratigraphy is color-mapped by the time of deposition, t^*. Stratigraphic vertical exaggeration = 50x, topographic vertical exaggeration = 0.05x.

Figure 5. Stratigraphic section from scenario 1, initial condition 6. Synthetic stratigraphy is color-mapped by the time of deposition, t^*. Stratigraphic vertical exaggeration = 100x, topographic vertical exaggeration = 0.05x.

Figure 6. Stratigraphic section from scenario 2, initial condition 6. Synthetic stratigraphy is color-mapped by the time of deposition, t^*. Stratigraphic vertical exaggeration = 100x, topographic vertical exaggeration = 0.05x.

Figure 7. Stratigraphic section from scenario 3, initial condition 6. Synthetic stratigraphy is color-mapped by the time of deposition, t^*. Stratigraphic vertical exaggeration = 100x, topographic vertical exaggeration = 0.05x.

Figure 8. A) average number of dunes that have passed by a grid node, n_d during early simulation time. B) During later simulation time, n_d increases at approximately a constant rate for all scenarios. C) n_s, the average number of bounding surfaces stacked vertically above each grid node, during early simulation time. D), During later simulation time, n_s exhibits significantly different behavior between the three sets of allogenic boundary conditions. E) The number of bounding surfaces per bedform visit per grid node, κ, plotted as a function of t^*

Figure 9. Each scenario is plotted as an ensemble of 12 simulation runs. The darker curves indicate the ensemble-averaged response, and the lower and upper edges of the shaded envelopes indicate the 10^{th} and 90^{th} cumulative percentile responses, respectively. A) Coefficient of variation of bedform height, $c_v = \sigma_h \mu_h^{-1}$, B) Mean set thickness, μ_{st}, and C) preservation ratio, $\omega = \mu_{st}\, \mu_h^{-1}$, plotted as a function of t^*. Note: logarithmic vertical axes. Each scenario is plotted as an ensemble of 12 simulation runs. The darker curves indicate the ensemble-averaged response, and the lower and upper edges of the shaded envelopes indicate the 10^{th} and 90^{th} cumulative percentile responses, respectively.

Figure 10. Preservation ratio, ω plotted as a function of c_v^2. t^* is color-mapped along each scenario. The last time step of each scenario is annotated as $t^* = 3$. Each scenario is plotted as an ensemble of 12 simulation runs. The darker curves indicate the ensemble-averaged response, and the lower and upper edges of the shaded envelopes indicate the 10^{th} and 90^{th} cumulative percentile responses, respectively. Note: logarithmic axes.

1

TABLES

Parameter	Value
A	0.1
B	3
D	0.2
p	0.4
Δt	1
Δx	10

Table 1: Values of parameters used in all simulations. Units are arbitrary.

Figure 1 - one column

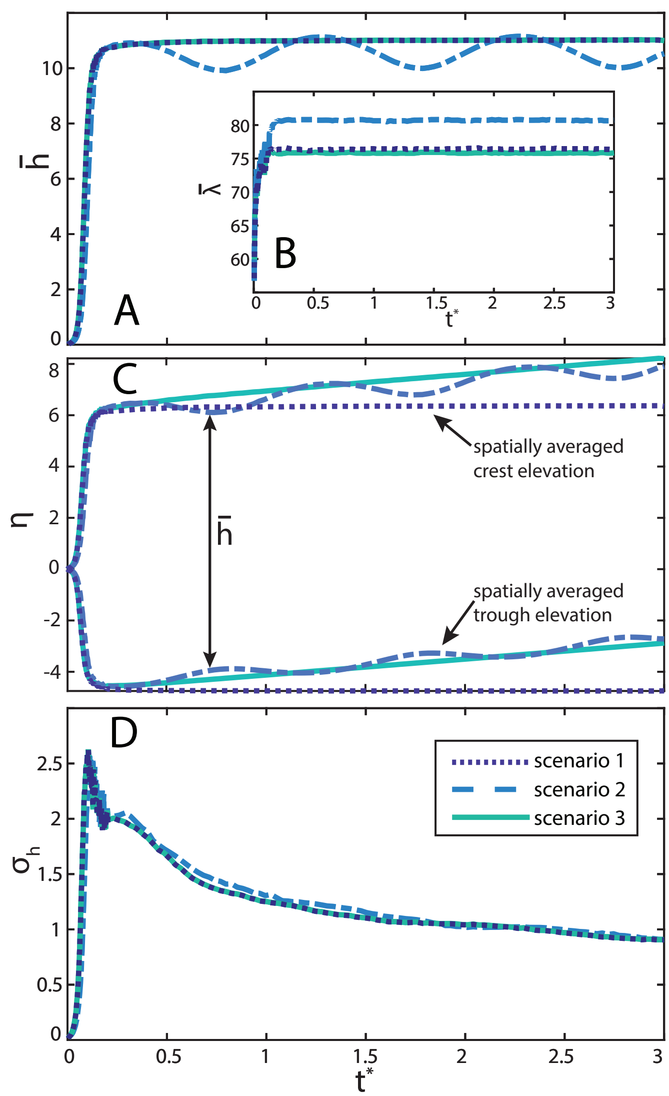

Figure 2 (2/3 page)

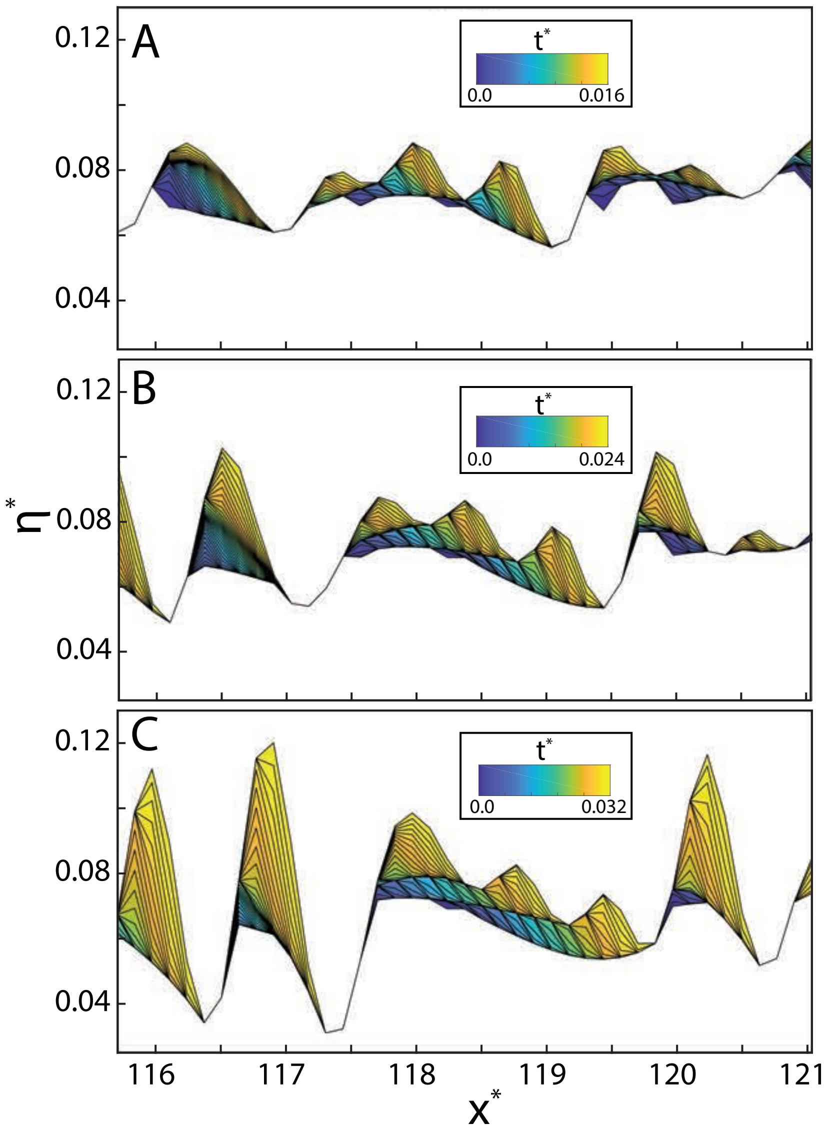

Figure 3 - 2/3 page

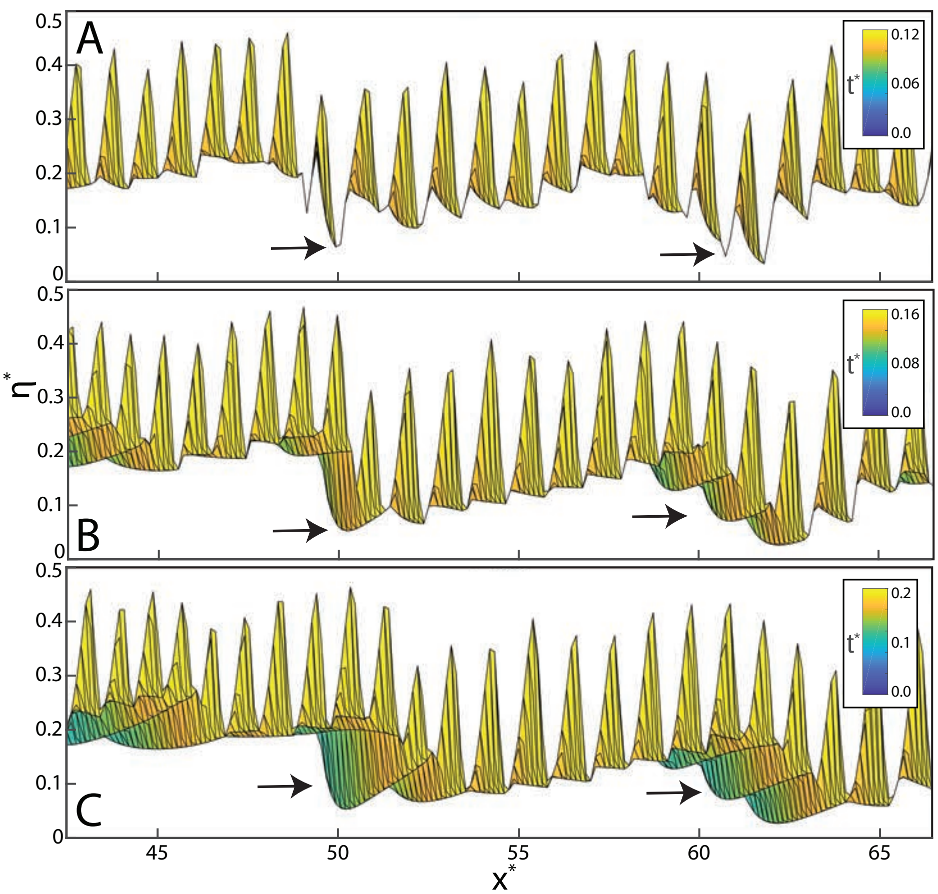

Figure 4 - 1 column

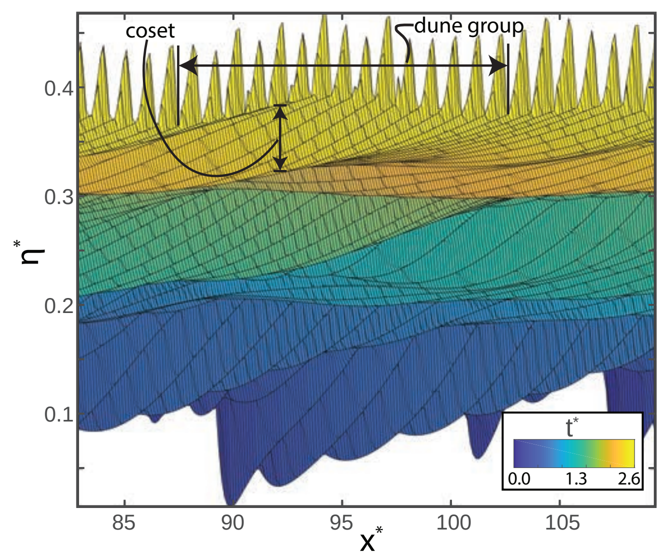

Figure 5 (landscape orientation - 1 column)

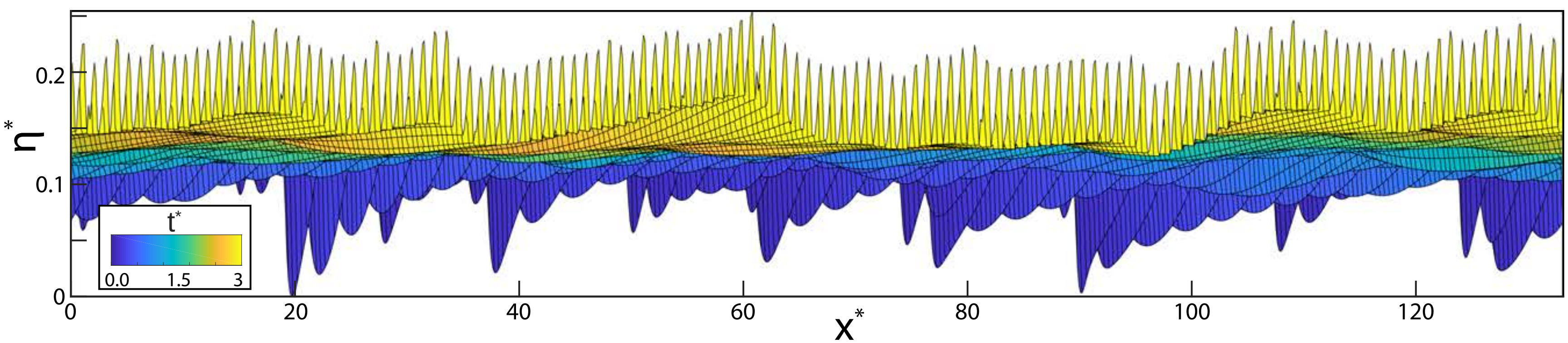

Figure 6 (landscape orientation - 1 column)

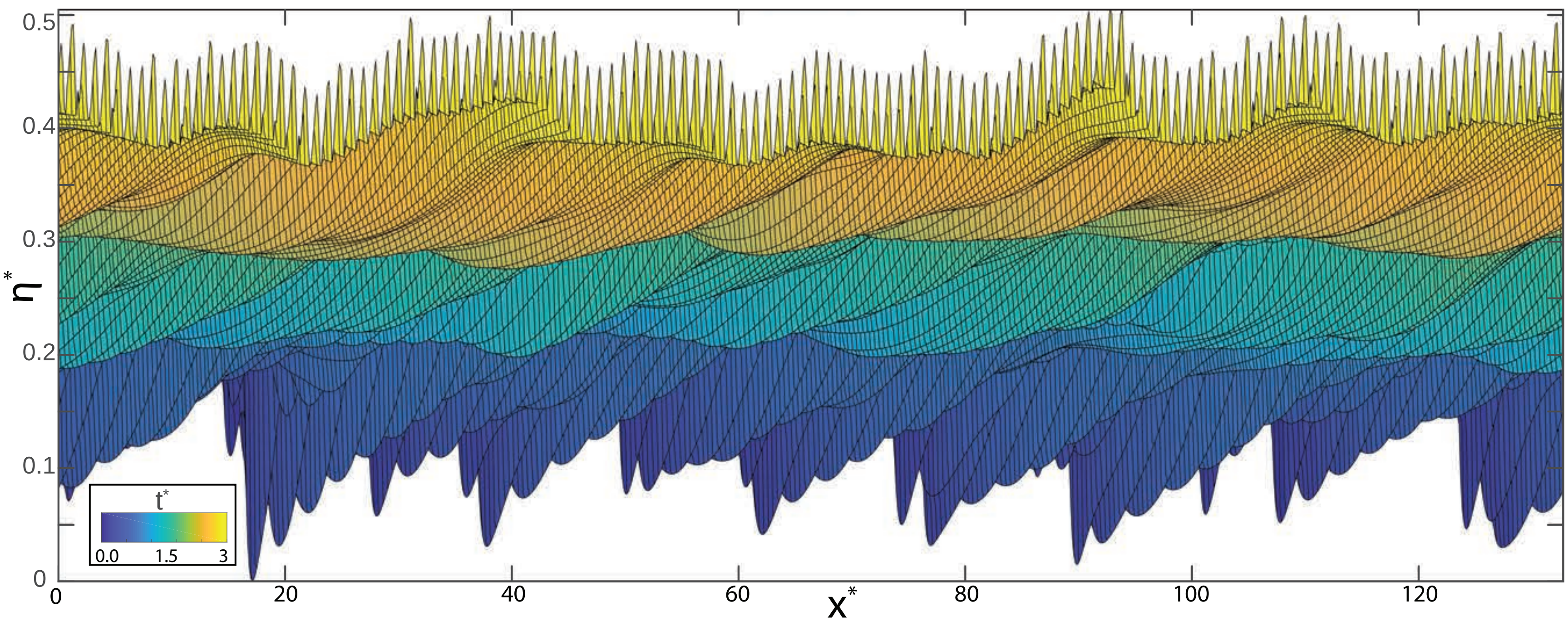

Figure 7 (landscape orientation - 1 column)

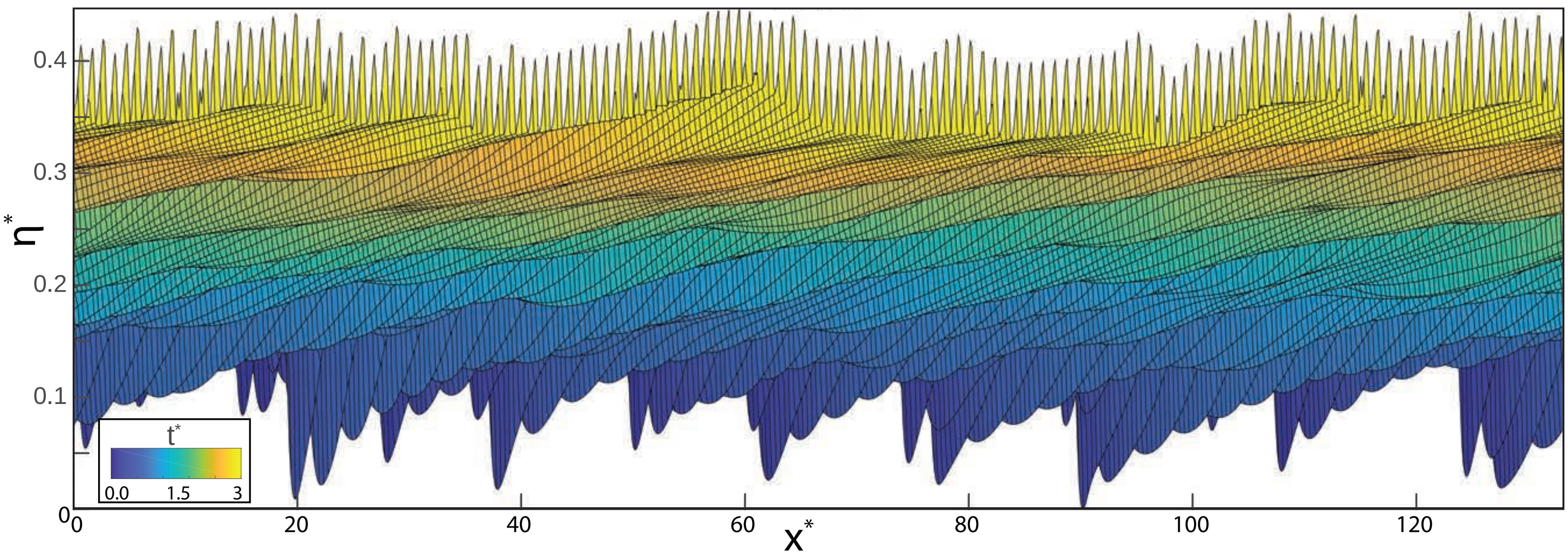

Figure 8 - one column

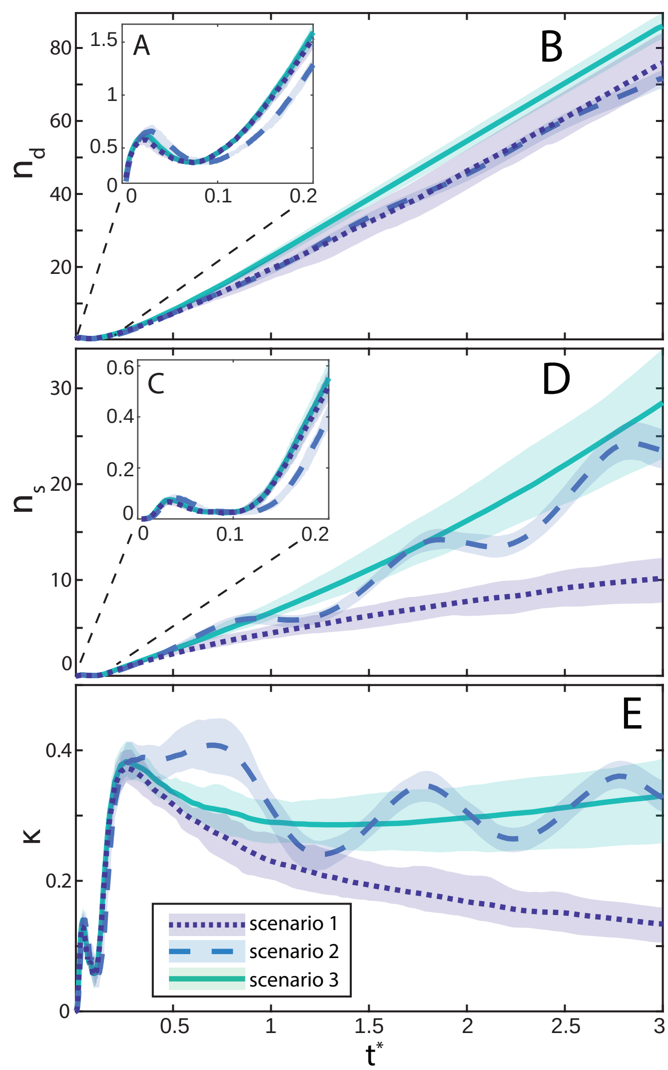

Figure 9 - one column

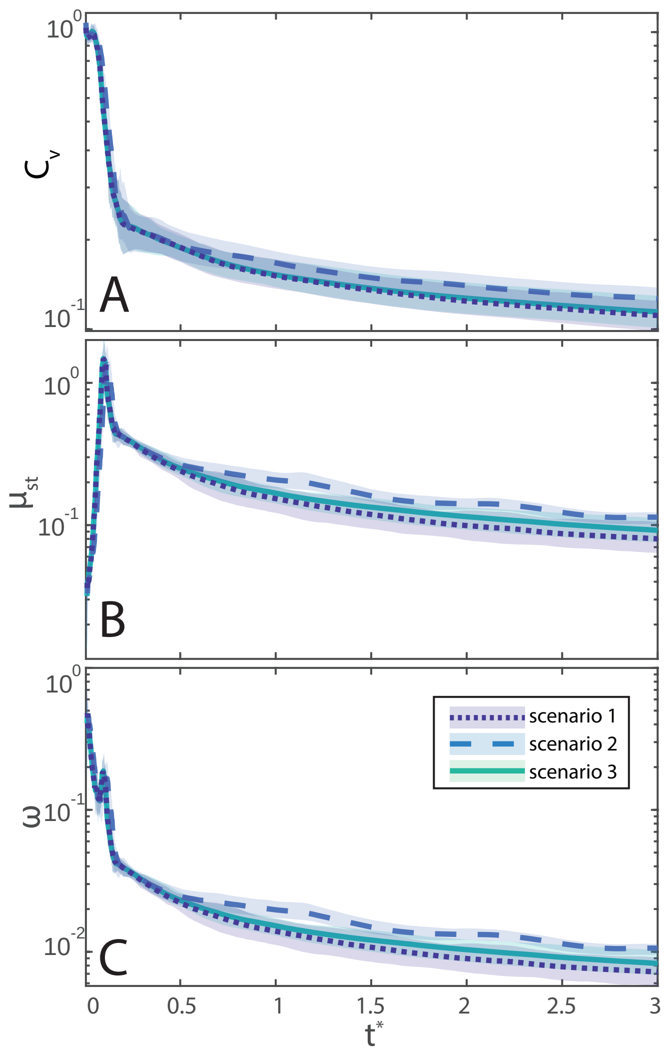

Figure 10 - 1 column

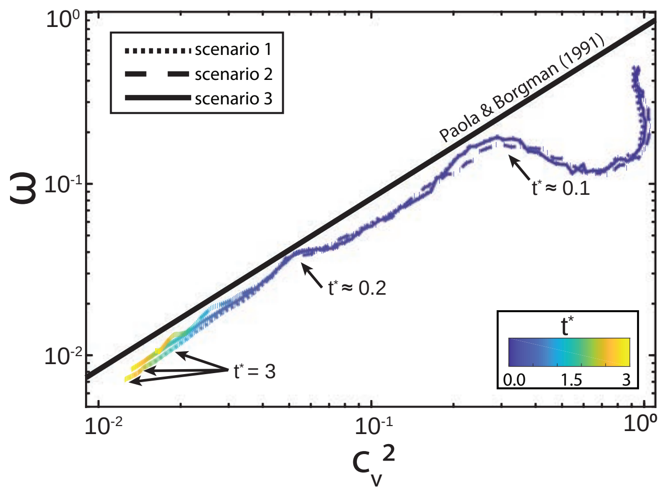

Supplementary Videos:

These videos will hopefully be hosted by the publisher. However, please review the videos via the three YouTube links below:

Scenario 1:

https://www.youtube.com/watch?v=Rkb1JJE2ToQ

Scenario 2:

https://www.youtube.com/watch?v=2Ru48Z4rjB4

Scenario 3:

https://www.youtube.com/watch?v=K1a_ceHRops